CHAPTER 5

Evaluation of Experimental Results

After the cyclic loading test in the experimental program, the test results were used to discuss and evaluate the seismic performance of the precast connections in an emulating monolithic behavior, compared to the monolithic concrete. Their performances, such as strength capacity, displacement ductility, stiffness degradation and energy dissipation, were adopted in seismic consideration.

5.1 Mode of failure

The location and type of failure of the concrete structure are very important for the structure in seismic region. Figure 5.1 illustrates the damages and failure modes of all test specimens after the cyclic loading test. These figures are given to compare and visualize the damage levels after the seismic ground motion.

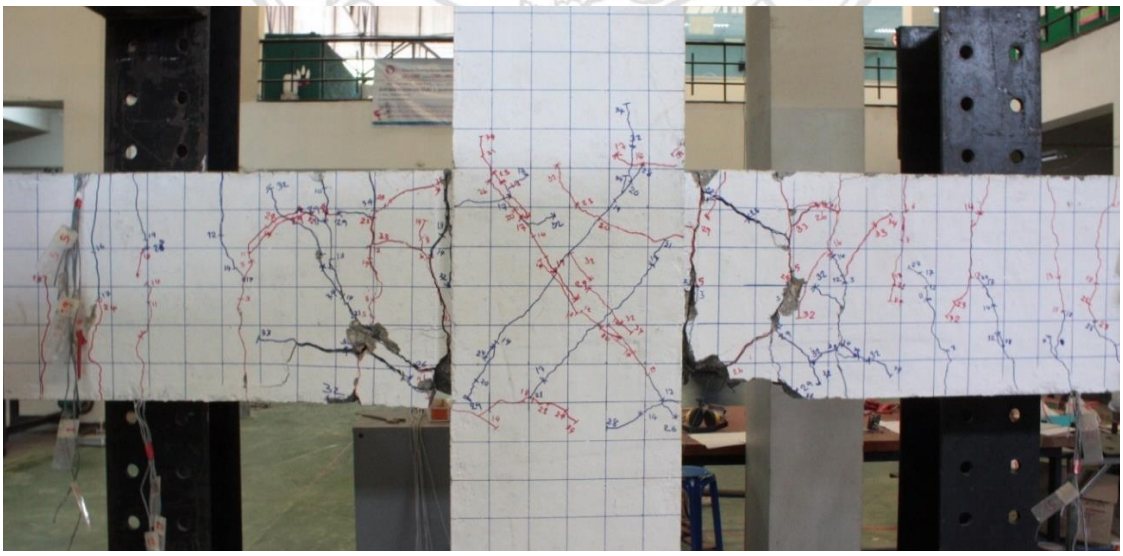

Figure 5.1 Crack distribution of monolithic specimen M1 at the end of testing

The cracking propagations of the monolithic specimen shown in Figure 5.1, is used as reference cracking pattern compared to other precast specimens. Because the strong

column-weak beam mechanism was performed to consider the concrete structural response in this study, most of flexural cracks were usually well distributed over the beams and there were a few flexural cracks appearing on the column elements. Furthermore, main diagonal cracks representing the strut mechanism within joint core were obviously investigated, meaning the bond problem of longitudinal beam reinforcement which was a few effects to a whole structural response. At the beam-ends, the plastic hinging region noticeably appeared at a distance of *d/2-d* from the column faces. Also, the concrete cover was spalled, causing a bulking of longitudinal reinforcement in the location.

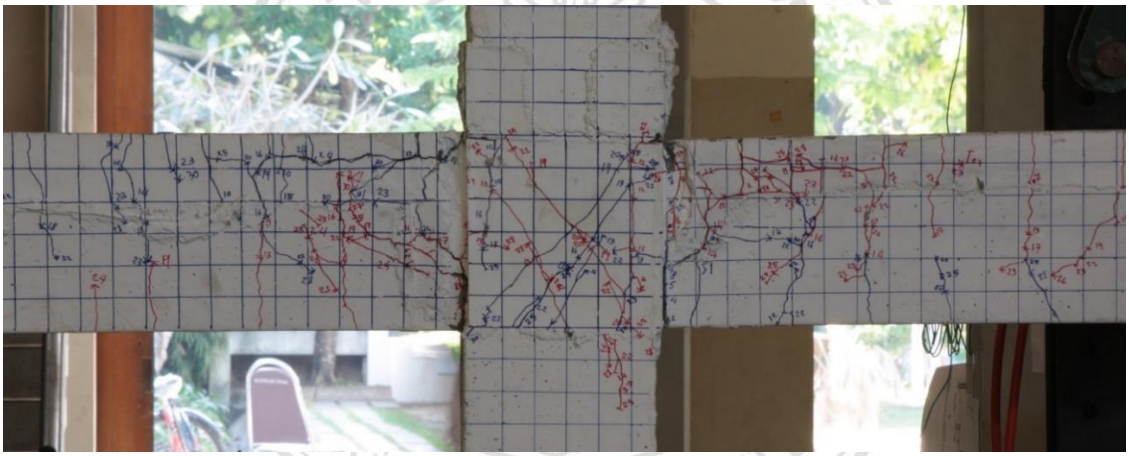

Figure 5.2 Crack distribution of precast specimen P1 at the end of testing

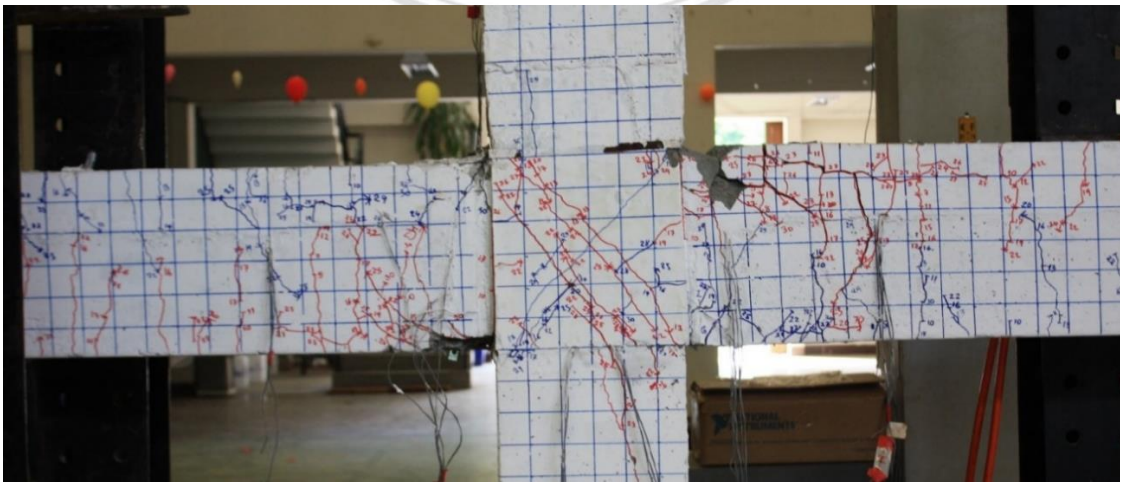

Figure 5.3 Crack distribution of precast specimen P2 at the end of testing

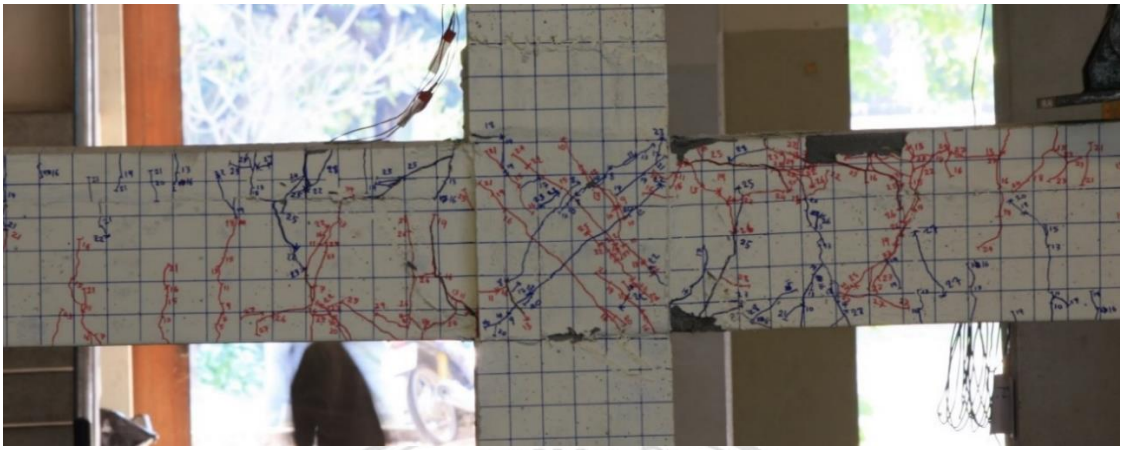

Figure 5.4 Crack distribution of precast specimen P3 at the end of testing

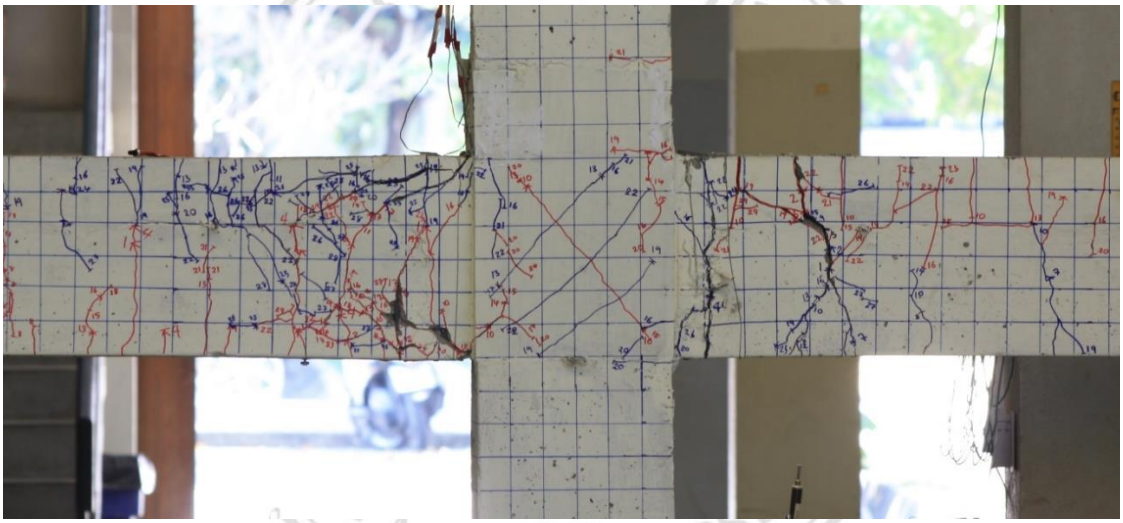

Figure 5.5 Crack distribution of precast specimen P4 at the end of testing

Due to the use of lap splice in the potential plastic hinging zones in precast specimens P1 to P4, the major failure mode progressed from tensile splitting-cracks, which developed along the splice length at the top of precast beam region in the non-shrink grout concrete region. That led to both slippage and strength degradation of the spliced reinforcement. The strength capacity rapidly decreased after the peak loading due to formation of longitudinal spitting cracks which was similar to the previous studies (Soroushian *et al.*, 1991 and Diab *et al.*, 2014) about bond behavior with high strength concrete. A number of flexural cracks were distributed over the precast concrete beams that were especially in the potential plastic hinge regions near the column. Moreover, several diagonal cracks on beam-column joint as shown in Figure 5.2 to Figure 5.5 were observed, exhibiting a combination of strut and truss mechanism under reversal cyclic displacement. Nevertheless, no crack appeared in both top and bottom columns of these

precast specimens. Regarding specimen P1 that used a chain-shaped bar to connect both precast beams, sliding of the T-sections that was observed during testing. There was no spalling of concrete cover significantly investigated during the experiment, while the concrete cover at the beam end regions of precast specimen P2-P4 were spalled. That means the internal compression force in the longitudinal bars of the P1 specimen which was less than the others, exhibiting by the specimen P1 which was lowest in terms of an external strength capacity.

For the precast connection details using boule T-section steels, the cracking distribution of the precast specimens P5 and P6 after cyclic testing show in Figures 5.1(f-g) which were very similar. The relocation of potential plastic region distinctly exhibited, taken away at around distance of *d* from the beam-column adjacent. At the location, spalling of concrete covers spreading on the side beam surface were ostensibly observed and little splitting cracks appeared. Almost all flexural cracks diffusely appeared over the precast beams. Furthermore, there were insignificantly flexural cracks observed in the precast columns. However, there were little difference in the damaging beam region between specimen P5 and specimen P6. In regard with a diagonally cracking pattern in the joint region, the main diagonal cracks representing the strut mechanism were evidently developed in the specimen P5, but there were several diagonal cracks in other, causing strut mechanism combining with truss mechanism.

Figure 5.6 Crack distribution of precast specimen P5 at the end of testing

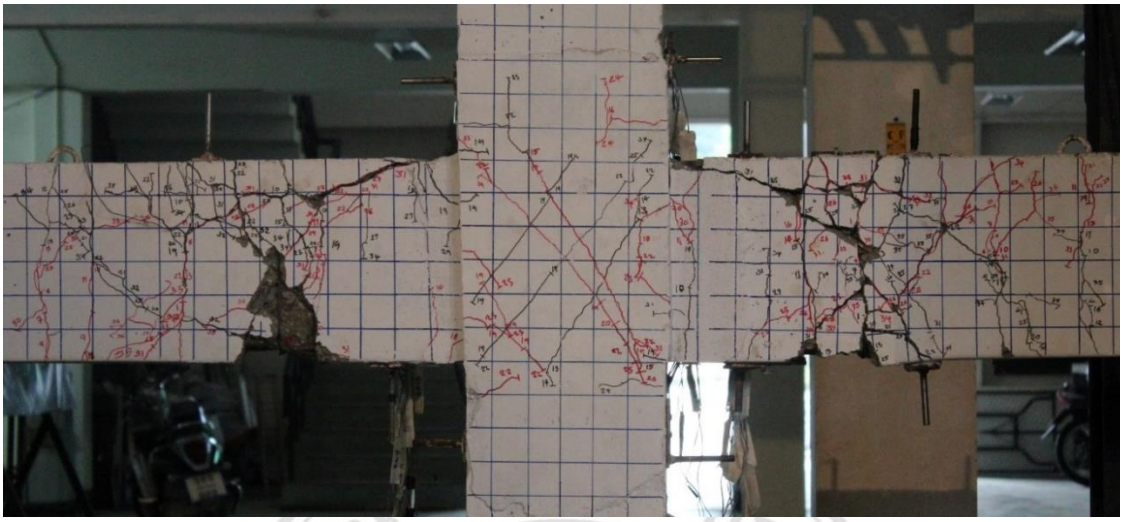

Figure 5.7 Crack distribution of precast specimen P6 at the end of testing

For bonding between high-strength grout concrete and normal concrete in all precast specimens, there were no instruments to observe the bond problem between existing concrete and non-shrink grout in the study. However, the crack pattern was observed during the test. There was no evidence in the bond-slip failure between the contacting areas.

5.2 Hysteresis behavior

The relationship of lateral load against displacement applying at the upper column for each specimen was shown in Figure 5.8. Figure 5.2(a) illustrates the lateral story shear and displacement hysteresis response of the monolithic specimen. Because no pinching effect was observed on the reversed response, the hysteresis behavior was good in terms of energy dissipation. The shear story showed little strength or stiffness degradation until the story drift level was up to 4.00%. Nevertheless, the degradation of maximum capacities in the repeating cycle was pronounced, less than the 0.85 times of the maximum strength in the first cycle at the same drift level. Plastic hinging took place in the beams at a distance of *d/2* from the column faces.

Regarding the P1 to P4 precast specimens, which have longitudinal lap splice bars at the top beam located at the beam end regions, a distance of *2d* from column faces. The hysteretic load-displacement relationships of the precast specimens P1-P4 are shown in Figure 5.2(b-e). As can be seen, the hysteresis response obviously exhibit the severely

pinching effect due to splitting crack in the top of the longitudinal lap splices and bond deterioration, indicating low energy dissipation. The widening of splitting cracks in high strength non-shrink region resulted in the dramatic degradation of story shear capacity after peak loading. These precast specimens showed a limited ductile response as shown in Fig. 10 (b) to Fig. 10 (e). The maximum lateral loads of these precast ones were presented in Table 5.1. The maximum loads of specimen P1 were lower than all the other precast specimens because the distance between main longitudinal bars and steel T-section were lower compared with the other precast specimens.

For the precast specimen P5, with double T-sections installed into the top and bottom beam region, located within distance *d* from column faces, behaved satisfactorily. The hysteresis behavior of the specimen showed a little pinching during the reversible load testing and the considerable pinching effect occurred in the precast specimen due to the observed flexural failure in the precast beams. The failure mode represents the successful relocation of the plastic hinge in the beams. However, there were a few splitting cracks appearing at the lap splice regions in precast beam. Behavior of this specimen was good in terms of ductility and energy dissipation when compared with previous precast ones. The column story shear versus drift ratio of the specimen P5 is shown in Figure 5.2(f), the envelope curve presented the strength degradation was rapid post peak strength due to bond deterioration.

The connection detail of precast specimen P6 were improved from the P5 precast connection, without lap splice for main longitudinal reinforcement in critical beam plastic hinging zone. The hysteresis response of the specimen was very similar to monolithic specimen M1. Throughout the cyclic displacement loading, no pinching effect was observed because of without the bond problem with this precast connection, leading to higher energy dissipating than other precast connections. For the envelope curve, there was a little strength degradation after the drift ratio up to 1.40% as shown in Figure 5.8 (g). However, the maximum strength in the repeating cycle was obviously dropped, less than the 0.85 times of the maximum strength in the first cycle at the 4.50% drift level.

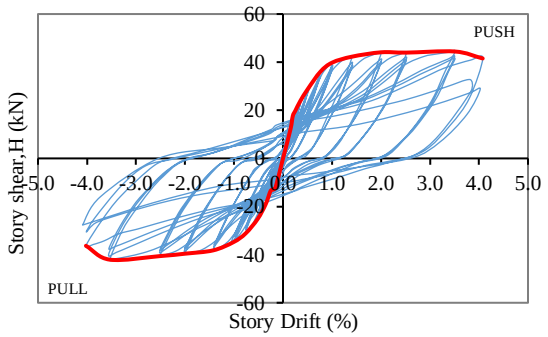

(a) Specimen M1

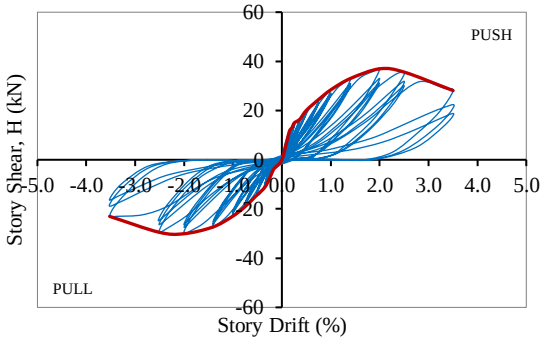

(b) Specimen P1

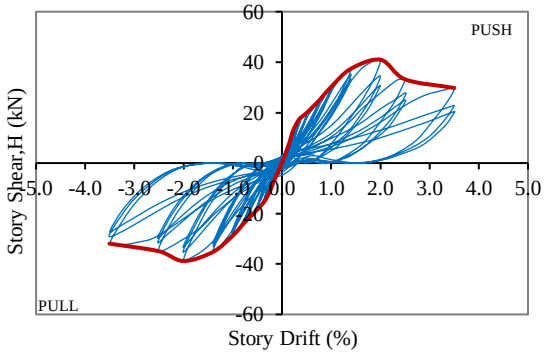

(c) Specimen P2

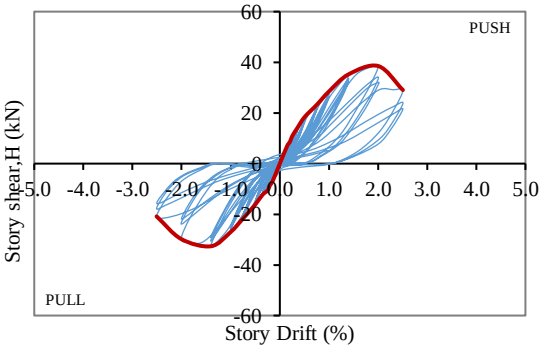

(d) Specimen P3

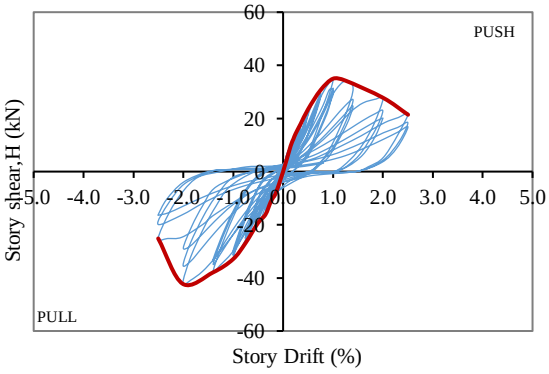

(e) Specimen P4

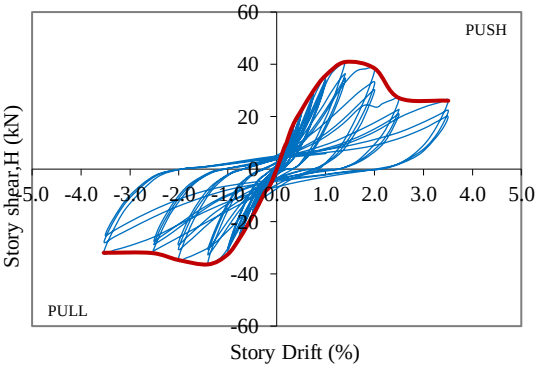

(f) Specimen P5

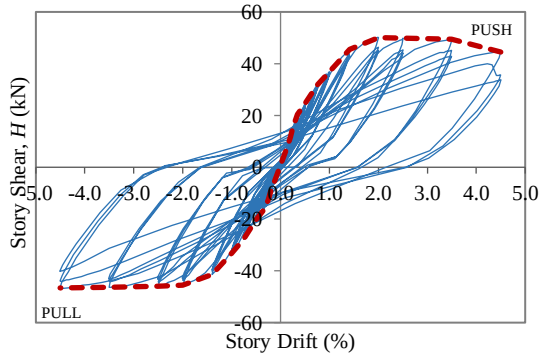

(g) Specimen P6

Figure 5.8 Story shear force vs. story drift ratio of test specimens

5.3 Strength capacity

Regarding ultimate strengths of all test specimens, the test result shows in Table 5.1. Furthermore, Figure 5.9 shows a strength comparison of precast and cast-in-place connections. Also, the normalized strength, ratio of story shear to strength capacities of M1 specimen, is another comparison strength from the experimental result as shown in Figure 5.10. Almost all precast connections had lower strength capacity than the monolithic one. Except P6 specimen, its maximum strength was higher due to the critical plastic hinge relocated away from the traditionally plastic hinging location same with other precast specimens.

Regarding a comparison between the strength capacities of the P2-P6 and P1 connection, it can be evidently seen that the improving and relocating connections, P2-P4 and P5-P6 specimens respectively, were better than the capacity of P1 specimen. Especially P6 specimen, its shear capacity was the largest due to an effect of the plastic hinge beam relocation without slippage. It can be concluded that all developed precast connections are successfully able to improve the story shear capacity better than the current precast connection.

In addition, the expected ultimate strengths according to the section capacity in the critical region were conveniently calculated to compare with the test result. It can be seen that the maximum strength of the monolithic specimen was very close with the expected ultimate strength. Because deterioration of bonding stress resulted in the slippage and splitting cracks along the lapped length in high strength non-shrink region appeared during experiment, the experimental ultimate capacities of P1 to P5 precast specimens were lower than the expected maximum strength and the average maximum strength of monolithic specimen. Excepting the test result of the P6 specimen, the strength capacity was better than the M1 monolithic connection and it was closely the expected maximum strength.

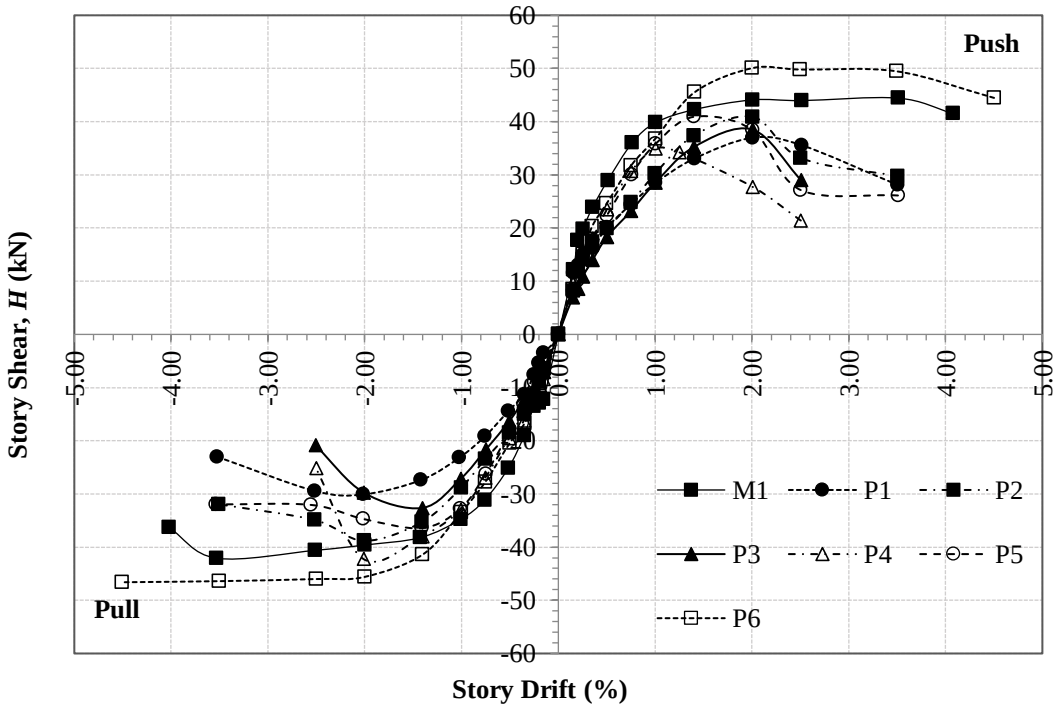

Figure 5.9 Comparison of backbone curves

Table 5.1 Ultimate strength and story drift level at peak of story shear

Specimen	Ultimate strength (kN)		Average Ultimate Strength (kN)	Expected Ultimate Strength (kN)	Ratio* of $\frac{H_{avg}}{H_{avg-M1}}$	Ratio** of $\frac{H_{avg-Pi}}{H_{avg-P1}}$	Ratio of $\frac{H_{avg}}{H_{expect}}$
	Push Side (H+)	Pull Side (*H*-)	H_{avg}	H_{expect}			
M1	44.43	42.08	43.25	43.25	1.00	-	1.02
P1	36.99	30.09	33.54	41.28	0.77	1.00	0.81
P2	40.91	38.81	39.86	33.42	0.92	1.19	1.19
P3	38.52	32.63	35.58	33.42	0.82	1.06	1.06
P4	34.98	42.23	38.61	33.42	0.90	1.15	1.16
P5	40.92	36.42	38.67	54.06	0.90	1.15	0.72
P6	50.07	46.60	48.34	54.06	1.12	1.44	0.89

* Ratio between average ultimate strength of corresponding specimen to monolithic control specimen (M1).

** Ratio between average ultimate strength of corresponding precast specimen (P_i) to P1 precast specimen (P1)

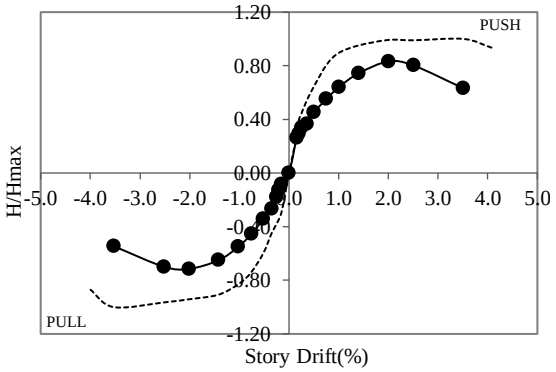

(a) Specimen P1

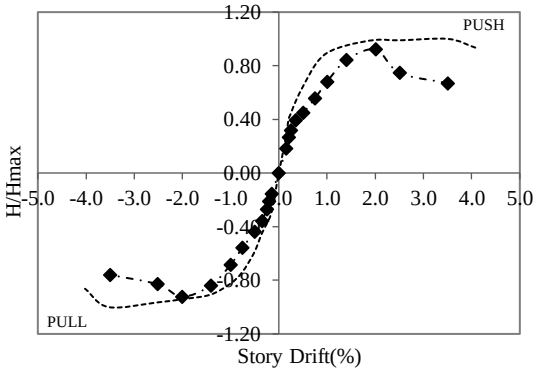

(b) Specimen P2

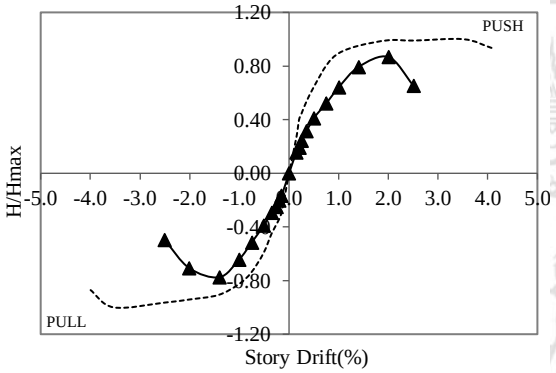

(c) Specimen P3

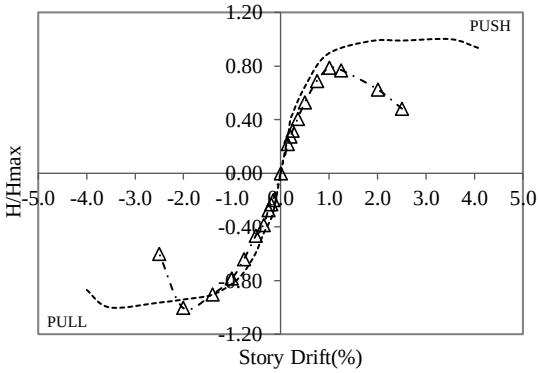

(d) Specimen P4

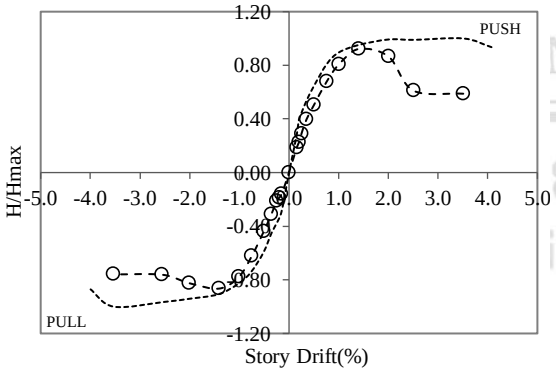

(e) Specimen P5

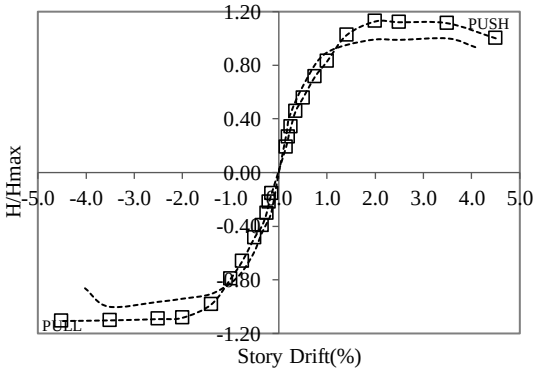

(f) Specimen P6

Figure 5.10 Backbone curves of the test specimens

5.4 Displacement ductility

The backbone curve of all specimens shown in Figure 5.9 was performed for conducting the strength and displacement ductility. As shown in Figure 5.11, the definition of equivalent yield (Δ_y). and ultimate displacement (Δ_u) as proposed by Park (1989) for the general case of lateral load-displacement responses was adopted in this study of the ductility factor. The ultimate displacement was taken as the post peak displacement with a 15 percent drop off in the maximum lateral load capacity, or the strength of the repeating cycle decreased over 15 percent of the first cycle. The use of the displacement ductility factor was used to represent the inelastic deformable of the structure during seismic loading.

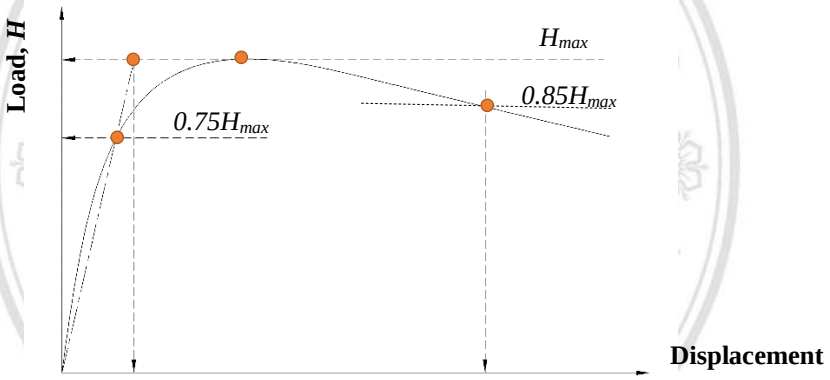

Figure 5.11 Definition for yield and ultimate displacements

Table 5.2 Displacement ductility factor

Specimen	Push Side			Pull Side			μ_{avg}
	Δ_u (%)	Δ_y (%)	μ	Δ_u (%)	Δ_y (%)	μ	
M1	4.00	0.90	4.44	4.00	1.00	4.00	4.22
P1	3.25	1.30	2.50	3.30	1.35	2.44	2.47
P2	2.45	1.35	1.82	3.50	1.35	2.60	2.21
P3	2.42	1.40	1.73	2.35	1.15	2.04	1.89
P4	1.75	0.78	2.24	2.28	1.28	1.78	2.01
P5	2.20	1.10	2.00	3.50	1.08	3.24	2.62
P6	4.50	1.38	3.26	4.50	1.40	3.21	3.24

* The 4.00+ means that the ultimate drift level was over 4.00% and the ductility factor was over 4.00.

The displacement ductility factors of all test specimens are shown in Table 5.2. The ductility factor of precast specimen P1, P2, P3 and P4 were similar. Because the major failure of these precast specimens were splitting cracks along lapped length of longitudinal reinforcement in high-strength grout region, the story shear were rapidly degraded after peak loading that was the main reason of a low ductility in these precast specimen. The precast specimen P5 and P6 were difference. The ductility factor of both specimen were better than the other precast specimens due to the potential plastic hinging region relocated away from the column faces. However, The P5 specimen was inferior to the P6 specimen. Because there were longitudinally splitting cracks at the edges of the T-section steels in the beam elements of the P5 specimen, leading to dramatic deterioration of the story shear after formation of the cracks. The overall behavior of P6 connection was very similar to monolithic connection, showing the best performance among the precast specimen. Nevertheless, the yield point of P6 specimen was greater than the conventional monolithic specimen as present in Table 5.2. Therefore, its ductility factor was 3.24, less than the monolithic one.

5.5 Stiffness degradation

In this study, stiffness degradation was discussed based on the secant stiffness, to observe the stiffness deterioration in each progressive drift level. The secant stiffness (K_{sec}) of any drift ratio at the last loading cycle or the third cycle, which was calculated from the peak of pulling side to the peak of pushing side, also called peak-to-peak stiffness, as shown in Figure 5.12, divided by the corresponding lateral displacement (d_1+d_2). The secant stiffness value for each drift ratio was normalized (K_{norm}) by the secant stiffness at the 0.15 percent story drift, the first drift level.

The test results as shown in Figure 5.13 reveal that the specimen M1 shows higher stiffness degradation compared to the precast specimens at the lower drift levels. However, the degradation rate is decreased for the precast specimens, the steel inserts increase the stiffness and control cracking well at a lower load, especially for the specimen P5 and P6. However, when the critical crack was presented, the capacity suddenly decreased along with stiffness degradation.

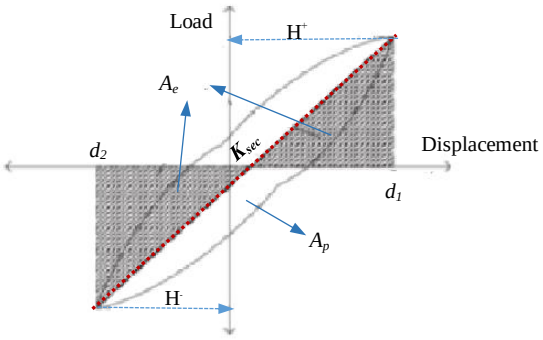

Figure 5.12 Secant stiffness and equivalent damping ratio

The stiffness degradation of specimens M1, P1, P2 and P5 are very similar, especially at higher levels of drift ratio. At the end of the last cycle, the loss of initial stiffness of the three specimens was approximately 10 -15 percent. For the precast specimens P3 and P4, the secant stiffness were dramatically dropped after the formation of the splitting cracks along lap-splices in the high strength grout region. The P6 specimen showed the best performance among all test specimens because the plastic beam hinges were successfully relocated from the column faces, especially without bond problem in this connection detail.

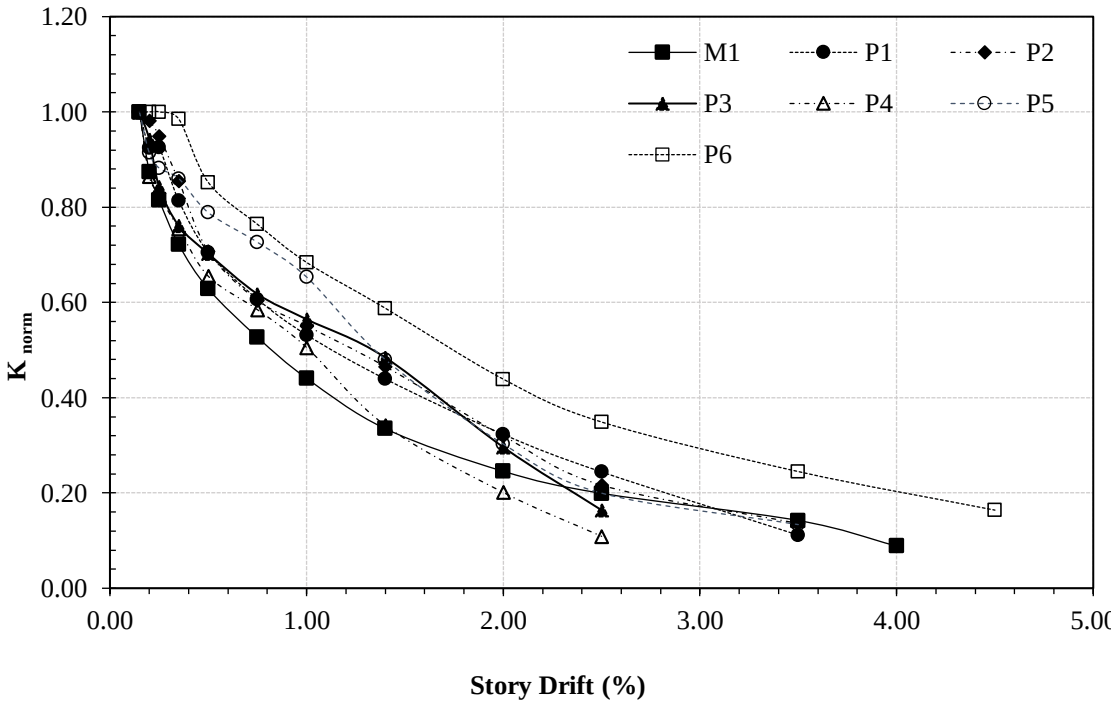

Figure 5.13 Stiffness degradation

5.6 Energy dissipation

In this study, the equivalent viscous damping ratio (ζ_{eq}) proposed by Chopra (2011) was widely used to explain energy dissipation characteristics. The equivalent-damping ratio was computed from the enclosed area within the hysteresis loop divided by strain energy, which is calculated from the assumed linear elastic behavior at corresponding cycles. This definition is formulated in equation (5.1).

$$\zeta_{eq} = \frac{1}{2\pi}\frac{A_p}{A_e} \times 100 \qquad (5.1)$$

The equivalent viscous damping ratio versus story drift level of all test specimens is shown in Figure 5.14. Especially higher drift level, the equivalent damping of the monolithic specimen M1 was higher than all the other precast ones. The equivalent damping response of the specimen P6 was similar to the M1 specimen; it also showed the best damping performance, comparing with the other precast. At higher drift level, precast specimens P1, P2, P3 and P4 were obviously very low due to a pinching effect during reversal movement, especially the P1 specimen designed mainly for gravity loading.

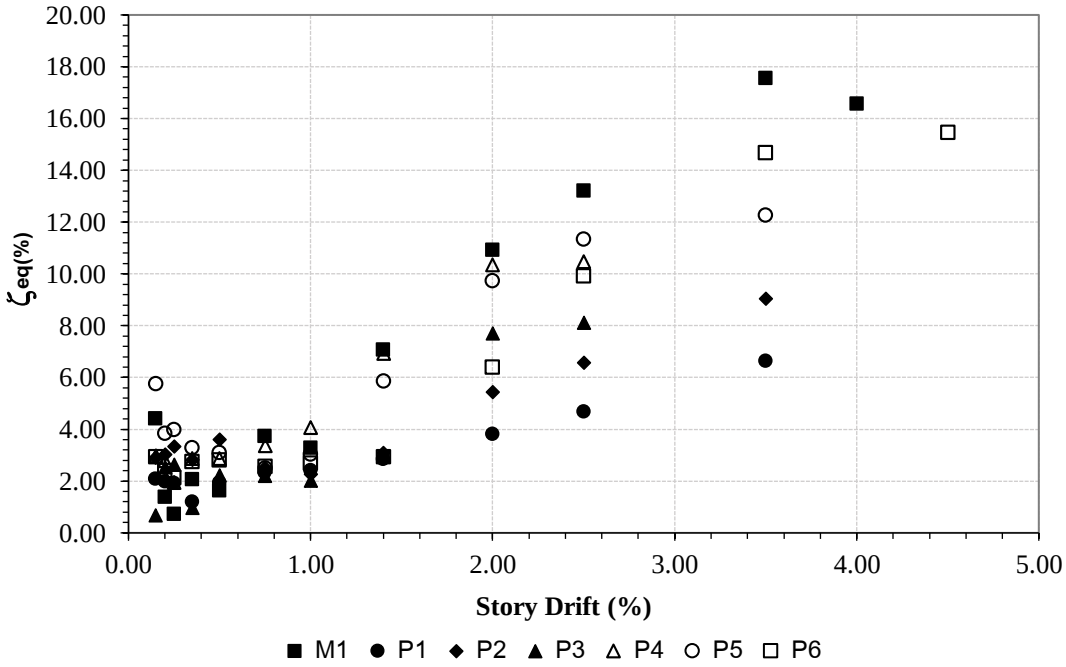

Figure 5.14 Equivalent damping ratio

5.7 Strain distribution

All specimens obviously exhibited a strong column-weak beam mechanism. Therefore, the longitudinal reinforcement of beam at top and bottom of the joint region were a critical location during experiment. The study explains the strain profiles at the story drift level 1.00% to 2.50%, the yield point and the ultimate point of most precast specimens, respectively. The stain profiles of the top and bottom reinforcement in the critical region at each the story drift level are explained in Figure 5.15 and Figure 5.16.

At the story drift level 1.00% as yield point of the test specimens, only reinforcement of monolithic specimen M1 rose to yield strain level. Also, the strain levels of top and bottom reinforcement of specimen M1 were up over the yield level at the beam plastic hinge zone, at 2.50% story drift. For precast specimens, the strain profiles of all precast specimens were under the yield level, at 1.00% drift level. For the stain levels of the top reinforcement compared to the yield strain of steel bar at the story drift level 2.50%, the P1 and P3 specimens were higher but the P2 and P4 specimens were lower. For the P5 precast connection, the strain levels were climbed to over the yield level both T-section steel and the embedded steel bar at the edge of the T-section. For bottom reinforcement with T-section steel insert of all precast specimens, the levels of the reinforcement were higher than the yield level. Regard to the P6 connection, the strain level of top and bottom reinforcement developed over the yield level at the drift level of 1.00% and 0.75, respectively. The peak strains of the top and bottom reinforcement are taken away at around distance of *d* (200-250 mm) from the beam-column adjacent. It can be concluded that the connection is successfully able to relocate the potential plastic beam region. For comparison between the P1 and P6 specimen, the strain levels in the joint region of P1 connection rose over the yield level, showing the inelastic response of the reinforcement within the joint core. On the other hand, the strain level of the P6 specimen was still in the elastic response.

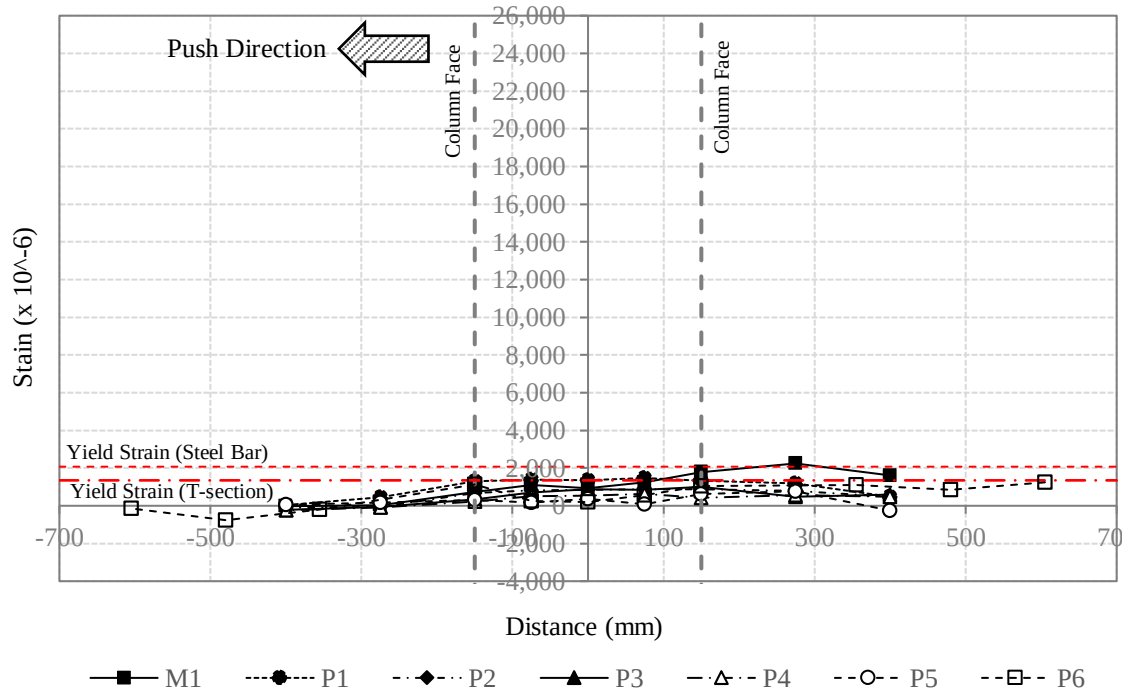

(a) Strain profile of Top reinforcement at +0.75% drift level (Push direction)

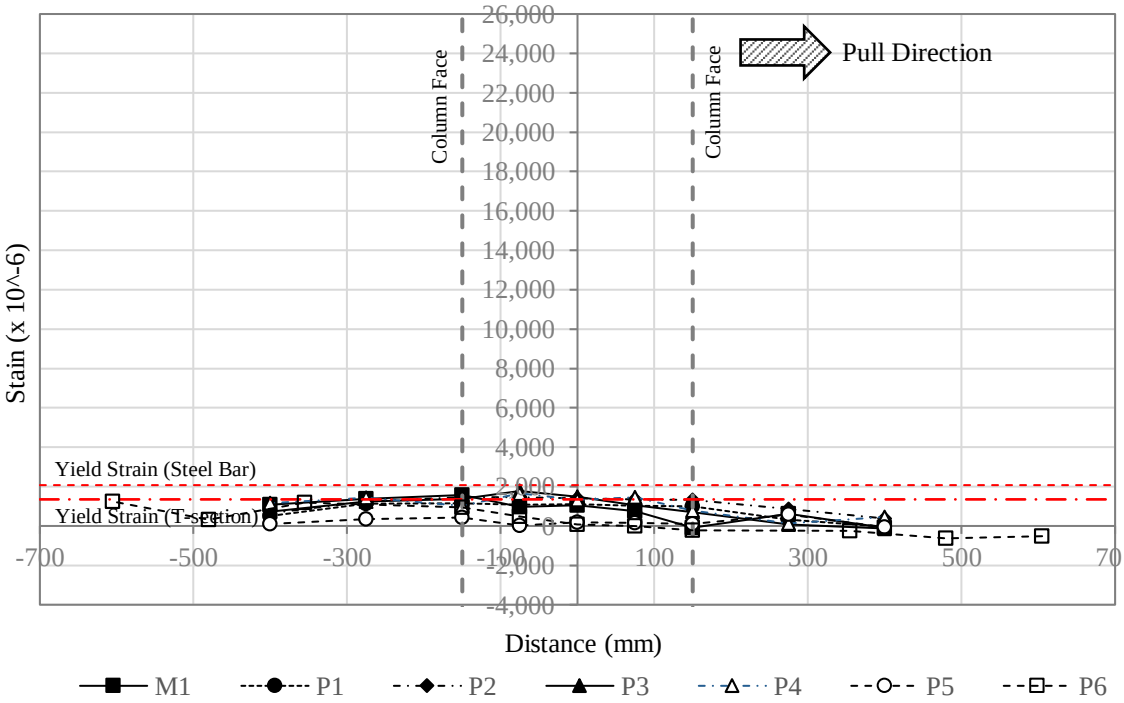

(b) Strain profile of Top reinforcement at -0.75% drift level (Pull direction)

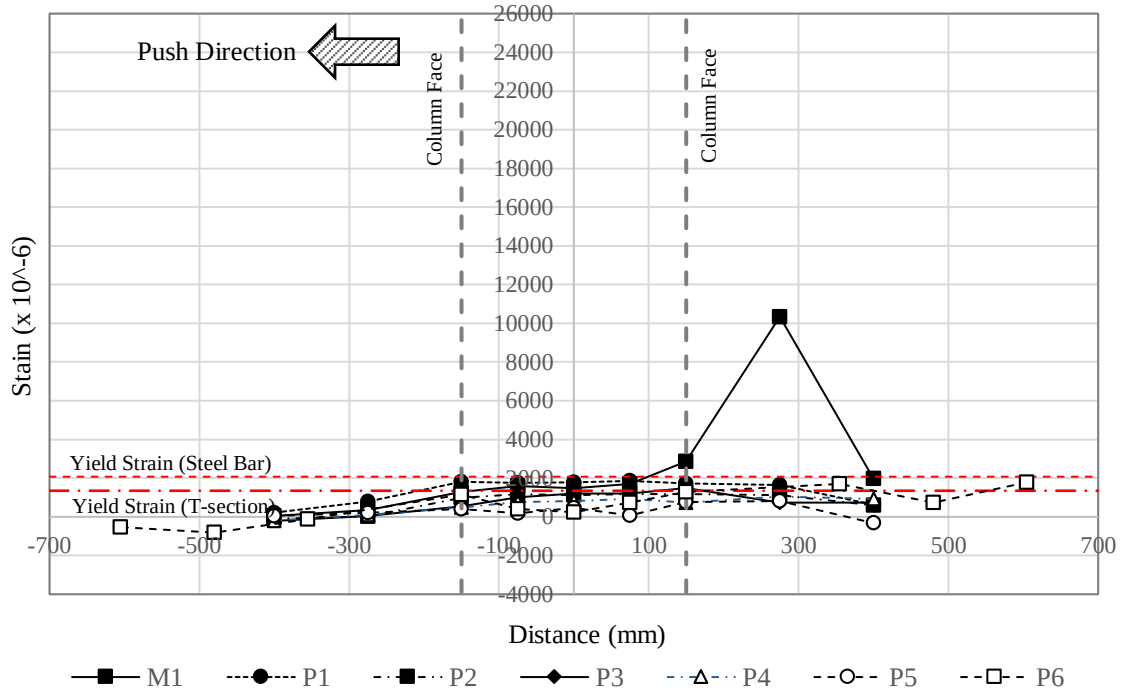

(c) Strain profile of Top reinforcement at +1.00% drift level (Push direction)

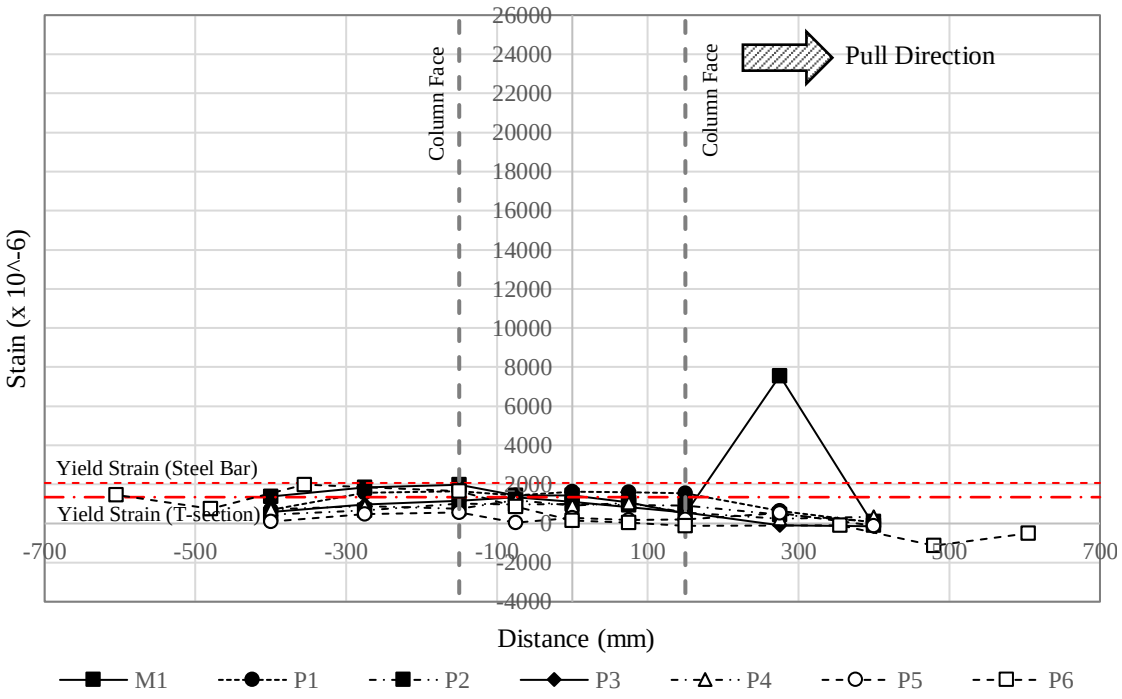

(d) Strain profile of Top reinforcement at -1.00% drift level (Pull direction)

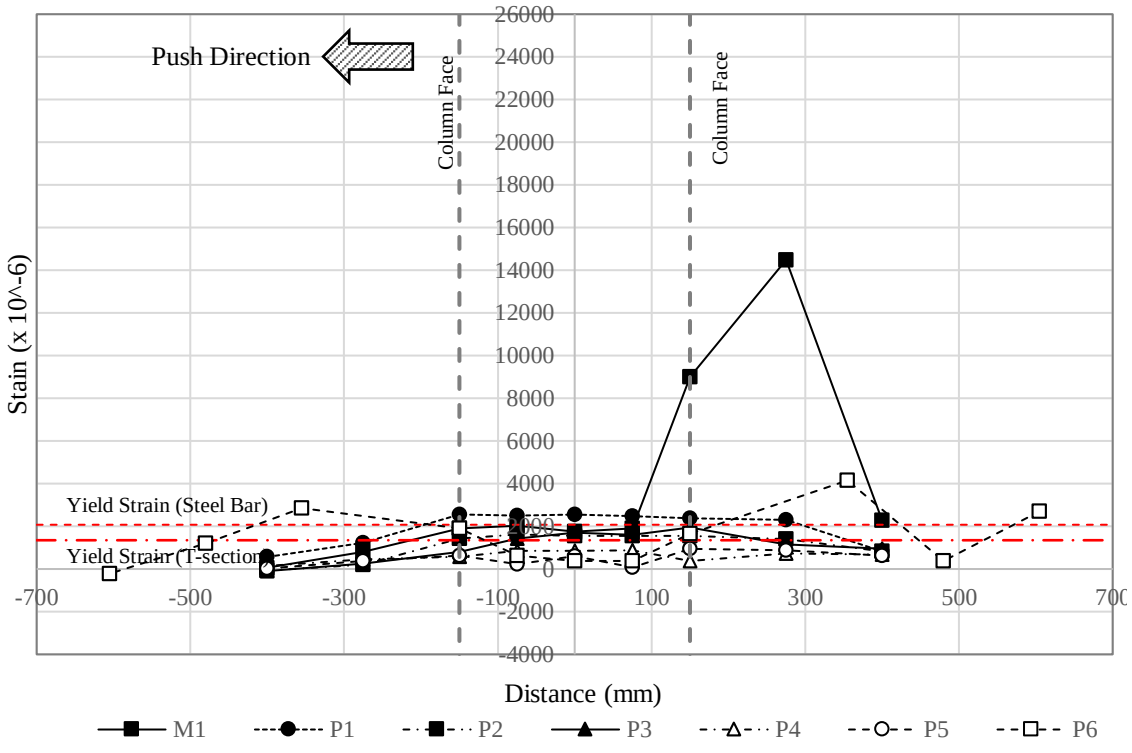

(e) Strain profile of Top reinforcement at +1.40% drift level (Push direction)

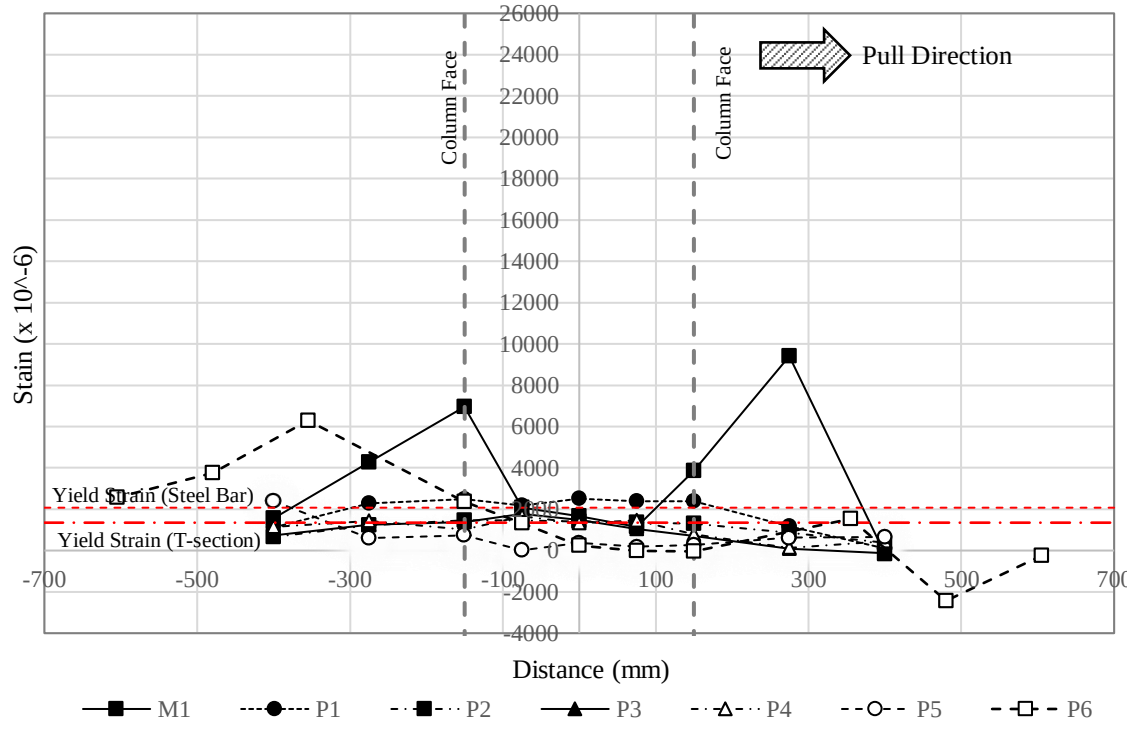

(f) Strain profile of Top reinforcement at -1.40% drift level (Pull direction)

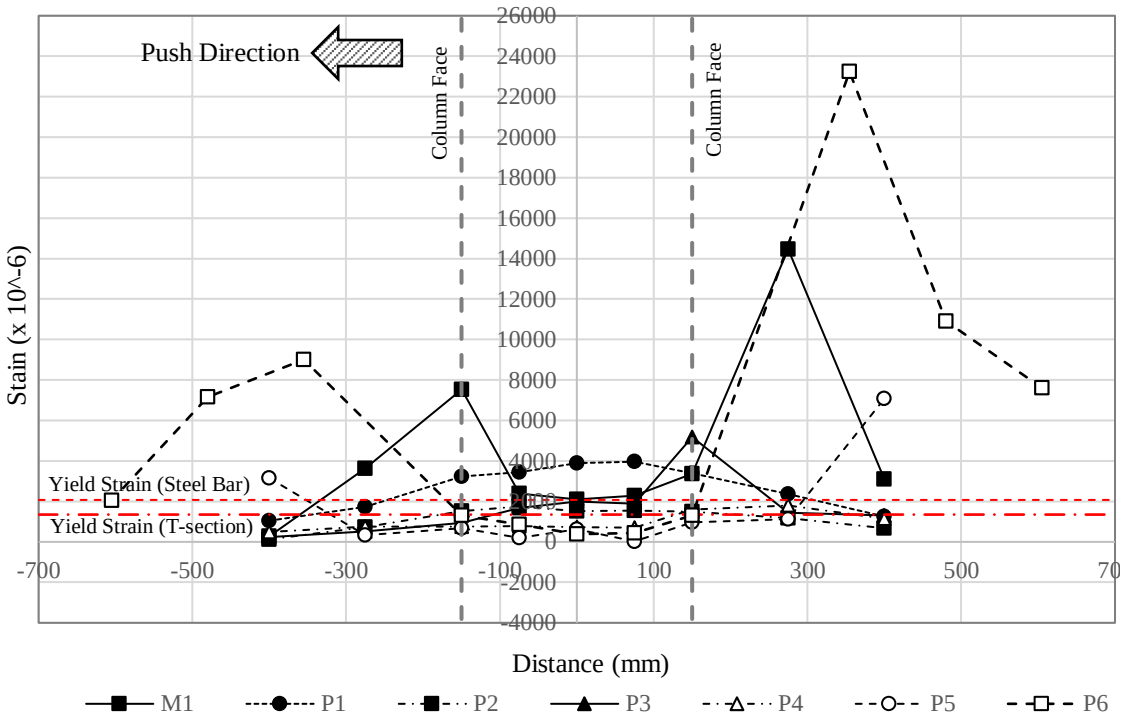

(g) Strain profile of Top reinforcement at +2.00% drift level (Push direction)

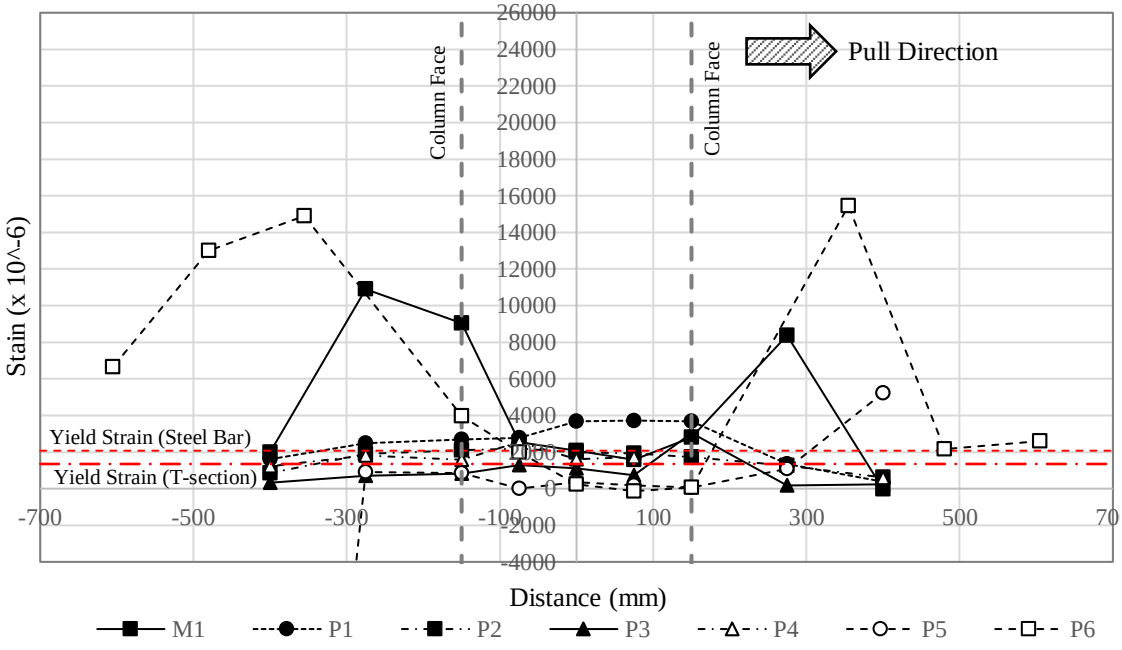

(h) Strain profile of Top reinforcement at -2.00% drift level (Pull direction)

Figure 5.15 Strain profile of top reinforcement

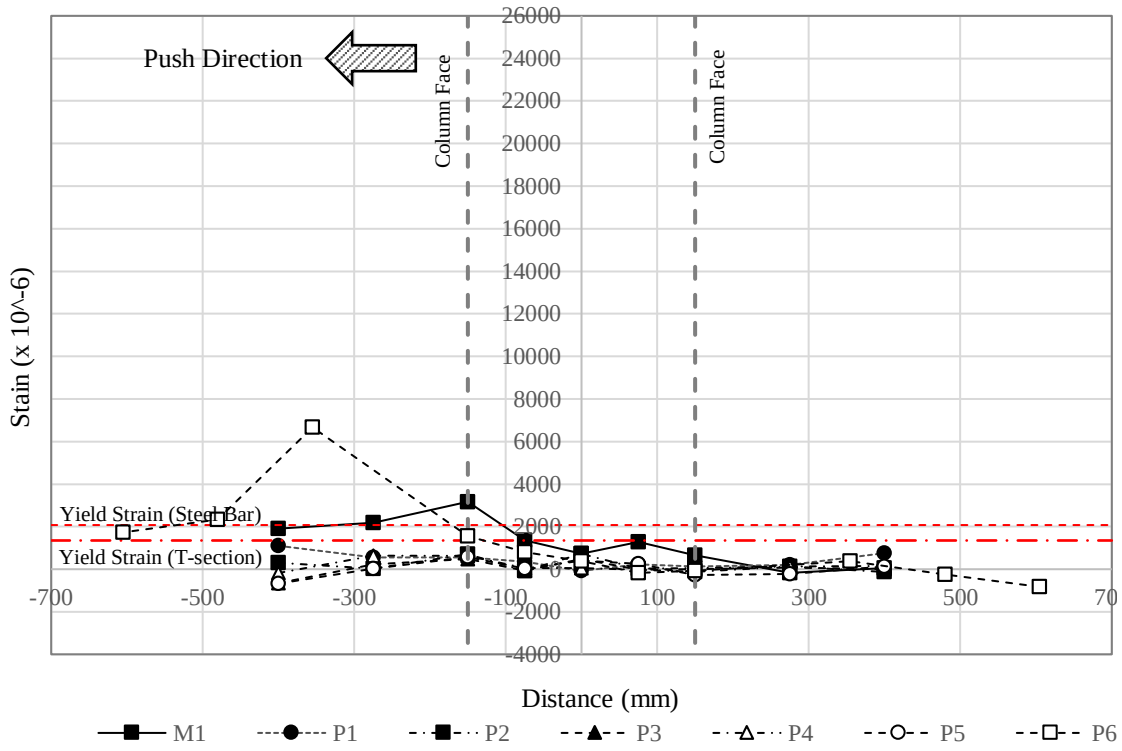

(a) Strain profile of bottom reinforcement at +0.75% drift level (Push direction)

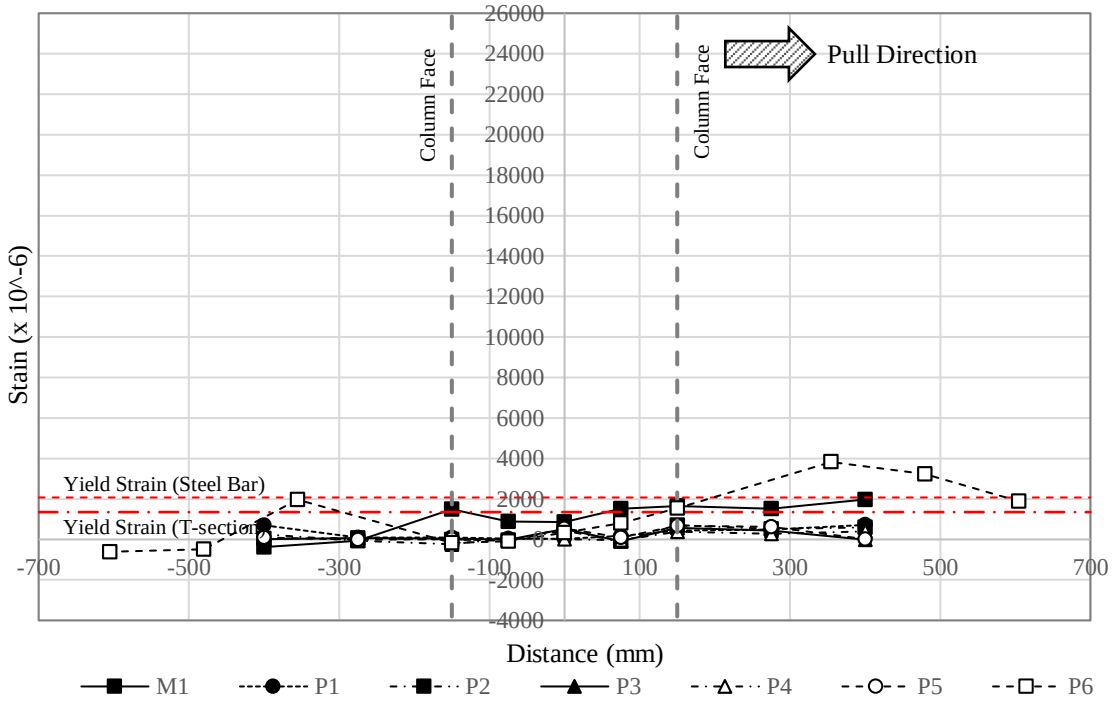

(b) Strain profile of bottom reinforcement at -0.75% drift level (Pull direction)

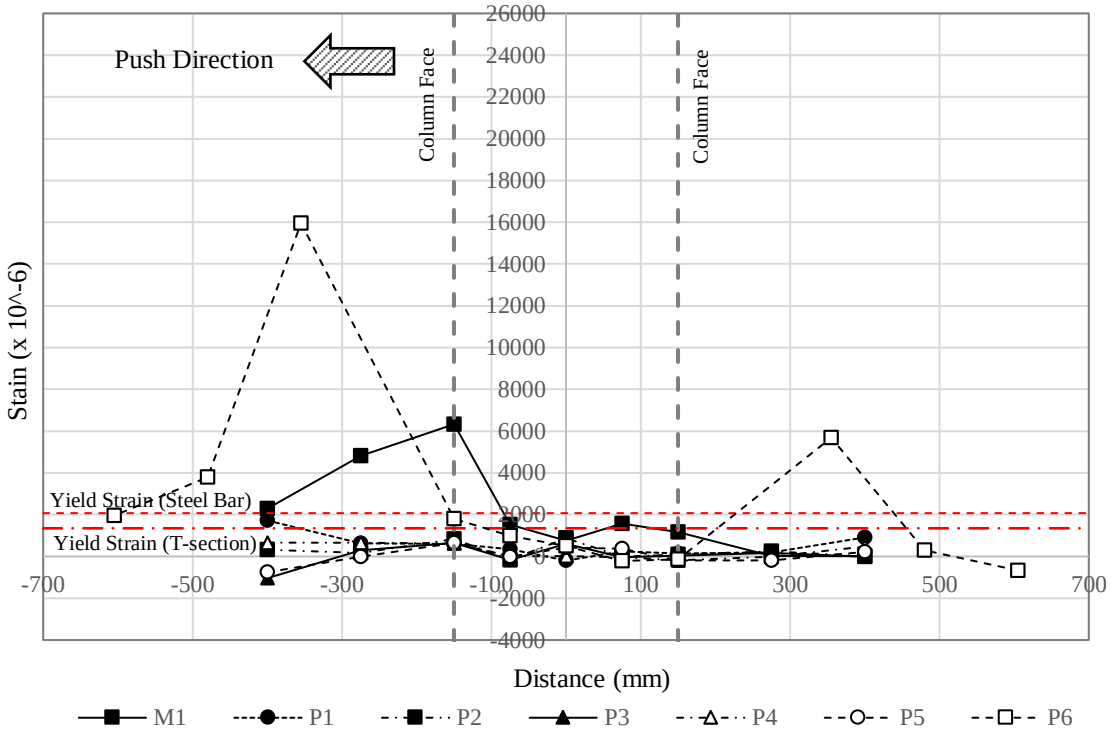

(c) Strain profile of bottom reinforcement at +1.00% drift level (Push direction)

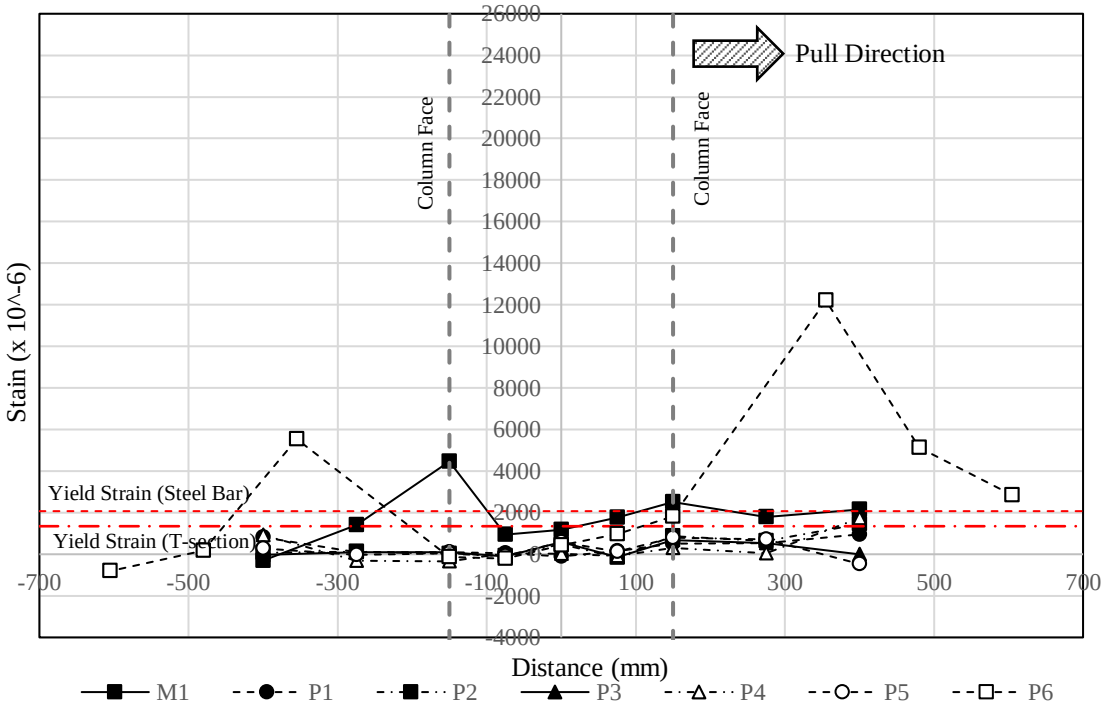

(d) Strain profile of bottom reinforcement at -1.00% drift level (Pull direction)

Figure 5.16 Strain profile of bottom reinforcement

5.8 Comparison material quantities and strength capacities of the precast connections

Table 5.3 and Table 5.4 show the comparison material quantities and strength capacities of the precast connections. All developed precast beam-to-beam connections (P2-P6) were compared the material quantities and average strength capacities to the current precast P1 connection. The material cost of P1 and P2 connections were the same but the loading capacity of P2 was higher than the current connection. The material costs of P3 and P4 connections comparing to the P1 connection were 1.12 and 1.41 times respectively. Likewise, the strength capacities were higher than the current specimen, 6% and 15% for the P3 and P4 connections respectively. For the P5 connection, the cost of steel reinforcement was lower but the strength capacity was 1.15 times larger than the current P1 connection. Although both costs of high-strength grout concrete and steel reinforcement of relocating P6 connection was the cheapest, its strength capacity was the greatest, 1.44 times of the P1 connection. It can be concluded that the developed P6 connection was better than the current P1 connection, both material cost and strength capacity.

Table 5.3 Comparison material quantities of the precast connections

Connection	Material					Normalization* of material quantities	
	Volume of grout concrete (cu.m)	Weight of steel reinforcement (kg)					
		Steel Plate, T-section steel (kg)	Lap-splice (kg)	Additional reinforcement (kg)	Total (kg)	Grout concrete	Steel reinforcement
P1	0.045	4.88	4.61	-	9.49	1.00	1.00
P2	0.045	4.88	4.61	-	9.49	1.00	1.00
P3	0.045	4.88	4.61	1.11	10.60	1.00	1.12
P4	0.045	4.88	4.61	3.93	13.42	1.00	1.41
P5	0.045	4.88	-	-	4.88	1.00	0.51
P6	0.028	3.99	-	-	3.99	0.62	0.42

* Normalization between material quantities of corresponding precast connections (P_i) to P1 current precast connection (P1)

Table 5.4 Summary of comparison material quantity and strength capacity of the precast connections

Connection	Normalization* of material quantities		Normalization* of Strength capacity
	Grout concrete	Steel reinforcement	
P1	1.00	1.00	1.00
P2	1.00	1.00	1.19
P3	1.00	1.12	1.06
P4	1.00	1.41	1.15
P5	1.00	0.51	1.15
P6	0.62	0.42	1.44